Vietnam Journal of Mechanics, Vol. 48, No. 1 (2026), pp. 94 – 104
DOI: https://doi.org/10.15625/0866-7136/23920

DYNAMIC INSTABILITY OF A DOUBLE CURVED SHALLOW SANDWICH ELECTROMAGNETIC SHELL WITH A THREE-PHASE NANOCOMPOSITE CORE

Pham Hong Cong[1], **Nguyen Van Huong**[2,3,*], **Nguyen Dinh Duc**[3], **Trinh Minh Chien**[4]
[1]*Centre for High Technology Research and Development, Vietnam Academy of Science and Technology, 18 Hoang Quoc Viet, Nghia Do, Hanoi, Vietnam*
[2]*University of Transport and Communications, 3 Cau Giay Street, Lang Ward, Hanoi, Vietnam*
[3]*VNU University of Engineering and Technology, Faculty of Civil Engineering, 144 Xuan Thuy, Cau Giay, Hanoi, Vietnam*
[4]*Department of Mechanical System Engineering, Jeonbuk National University, 567, Baekje-daero, Deokjin-gu, Jeonju-si, Jeollabuk-do, 54896 Republic of Korea*
E-mail: huongnv@utc.edu.vn

Received: 22 December 2025 / Revised: 5 January 2026 / Accepted: 10 January 2026
Published online: 10 March 2026

Abstract. This study examines the dynamic instability region (DIR) of a double-curved shallow sandwich electromagnetic (DSEM) shell containing a three-phase nanocomposite core and supported by an elastic foundation. The governing equations for nonlinear dynamic stability are formulated using first-order shear deformation theory (FSDT) combined with von Kármán geometric nonlinearity. The Galerkin method is applied to derive the nonlinear ordinary differential equations, and Bolotin's method is used to identify the DIR of the shell structure. Parametric analyses are conducted to evaluate the influences of electromagnetic fields, shell geometry, and core material properties on the nonlinear DIR.

Keywords: double curved shallow sandwich electromagnetic shell, nonlinear dynamic stability, three-phase nanocomposite, dynamic instability region.

1. INTRODUCTION

The multilayer double curved shell structure is widely used in various engineering fields, including civil infrastructure, aerospace, and marine systems. Consequently, issues related to its dynamic stability and dynamic response have become an active and important research topic. Among these, the free-vibration behavior and dynamic responses of double curved shallow shells have received particular attention. For example, static and vibration analyses of double curved shells with functionally graded (FG) face sheets and isotropic cores have been conducted using higher-order equivalent single-layer shell theories that incorporate shear stress and rotational inertia effects (Sayyad et al., 2023). Cong et al. (2024) investigated the dynamic response of double curved shallow nanoshell within the framework of nonlocal elasticity theory. In addition to analytical and conventional numerical approaches, the isogeometric analysis (IGA) method has also been employed to model and evaluate the free and forced vibration characteristics of magneto-electro-elastic (MEE) double curved shallow shells resting on a visco-Pasternak foundation under humid and elevated-temperature conditions (Tu et al., 2024).

Building upon these developments, recent studies have focused on improving the stiffness and multifunctionality of shell structures through the integration of advanced reinforcing materials. Van Huong et al. (2024) examined the free vibration behavior of a three-layer double curved shallow shell composed of electromagnetic outer layers and a three-phase nanocomposite core made of fibers, a polymer matrix, and carbon nanotubes or graphene platelets. Similarly, Anh et al. (2023) investigated the vibration characteristics of shells incorporating an auxetic core and FG face layers strengthened by a rib-stiffening system. These efforts highlight the growing interest in designing high-performance composite and nanocomposite shells capable of exhibiting enhanced mechanical, dynamic, and multiphysical responses.

Research on dynamic stability further supports the development of safer and more reliable structures by identifying critical dynamic load levels and determining instability regions under realistic operating conditions. For instance, nonlinear and chaotic instabilities of FG double curved shallow shells resting on a viscoelastic Hetényi foundation and subjected to combined in-plane and transverse excitations have been explored using third-order shear deformation theory (Jahangiri et al., 2022). Feng et al. (2024) analyzed the instability behavior of multilayer cylindrical shells immersed in fluid and demonstrated that an increase in excitation frequency corresponding to the dynamic instability region enhances structural dynamic stability. Despite these advances, most existing studies have primarily addressed vibration and dynamic response characteristics, with limited attention to the nonlinear dynamic stability of double-curvature sandwich shells featuring multifunctional material configurations.

Numerous studies have been conducted to analyze the dynamic instability and vibration response of complex composite structures using Bolotin's method (Bolotin, 1964). Yadav et al. (2022) performed a dynamic instability vibration analysis of multilayer composite cylindrical shells subjected to periodic boundary loads, with or without damping, based on the higher-order shear deformation theory (HSDT). Continuing the HSDT approach, they extended it to the analysis of dynamic instability and nonlinear vibrations of fluid-filled angle-ply composite cylindrical shells subjected to harmonic axial force (Yadav et al., 2023). Chakraborty et al. (2021) studied the parametric instability of functional gradient CNTRC composite cylindrical panels with damping in a thermal environment based on HSDT and von Kármán geometric nonlinearity, considering Rayleigh damping. Zaidan and Hasan (2023) conducted a comprehensive study on the dynamic instability of rotating functionally graded porous cylindrical panels under periodic axial loading, based on the FSDT with explicit consideration of Coriolis acceleration effects. Thi et al. (2025) studied the dynamic instability of porous metal nanosheets impregnated with piezoelectric fluids in a humid-thermal environment using the nonlocal strain gradient theory combined with the refined high-order shear strain theory.

In this study, for the first time, the nonlinear dynamic stability of a double curved shallow sandwich shell with a three-phase nanocomposite core and electromagnetic face layers is systematically investigated. The critical dynamic load is determined, and the corresponding dynamic instability region is established, providing valuable insight into optimizing the dynamic performance of such advanced shell structures.

2. BASIC EQUATIONS

2.1. The geometric shape and material properties

Fig. 1 illustrates a double curved shallow sandwich shell of length a and width b, defined with respect to the $Oxyz$ coordinate system, where the $x-y$ plane coincides with the shell's middle surface. The structure consists of three layers: a core layer of thickness h_2, composed of a three-phase composite material comprising a resin matrix, fibers, and nanofillers in the form of carbon nanotubes (CNTs) or graphene nanoplatelets (GPLs); and two outer electromagnetic face layers, each of thickness h_1. The shell rests on an elastic foundation characterized by the Winkler modulus k_1 and the Pasternak shear parameter k_2.

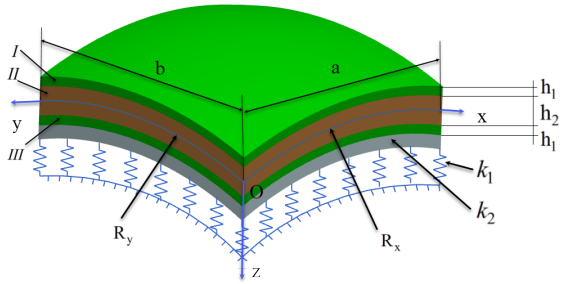

Fig. 1. The model of a double-curved shallow sandwich electromagnetic shell with a three-phase nanocomposite core on the elastic foundation

Based on the Halpin-Tsai model, the effective mechanical properties of the CNT/GPL-reinforced resin matrix are given as follows (Mirfatah et al., 2022):

$$\frac{E_r^c}{E_n}=\frac{3}{8}\left(\frac{1+2A_c\beta_L^cV_c}{1-\beta_L^cV_c}\right)+\frac{5}{8}\left(\frac{1+2\beta_T^cV_c}{1-\beta_T^cV_c}\right),\quad \frac{E_r^g}{E_n}=\frac{3}{8}\left(\frac{1+2A_g\beta_L^gV_g}{1-\beta_L^gV_g}\right)+\frac{5}{8}\left(\frac{1+2B_g\beta_T^gV_g}{1-\beta_T^gV_g}\right),$$
$$v_r^i=v_iV_i+v_n\left(1-V_i\right),\rho_r^i=\rho_iV_i+\rho_n\left(1-V_i\right),$$
$$\frac{\alpha_r^i}{\alpha_n}=\frac{1}{2}\left[\frac{V_iE_i\left(\alpha_i/\alpha_n\right)+V_nE_n}{V_iE_i+V_nE_n}\left(1-v_r^i\right)+V_i\left(1+v_i\right)\frac{\alpha_i}{\alpha_n}+V_n\left(1+v_n\right)\right], \tag{1}$$

where $i=c,g$, and

$$\beta_L^c=\frac{l_{cn}-A_c/4}{l_{cn}+B_c/2},\quad \beta_T^c=\frac{l_{cn}-A_c/4}{l_{cn}+A_c/2},\quad A_c=\frac{d_c}{h_c},\quad B_c=\frac{l_c}{h_c},\quad A_c=\frac{l_c}{d_c},\quad l_{cn}=\frac{E_c}{E_n},$$
$$\beta_L^g=\frac{l_{cg}-1}{l_{cg}+2A_g},\quad \beta_T^g=\frac{l_{cg}-1}{l_{cg}+2B_g},\quad A_g=\frac{l_g}{h_g},\quad B_g=\frac{w_g}{h_g},\quad l_{cg}=\frac{E_g}{E_n}, \tag{2}$$

in which the parameters E_i, v_i, α_i, ρ_i and V_i denote Young's modulus, Poisson's ratio, coefficient of thermal expansion, mass density, and volume fraction of CNTs and GPLs, respectively. The superscripts c and g correspond to CNTs and GPLs, respectively. Subscripts r and n refer to the reinforced nanocomposite matrix and the unreinforced resin matrix, respectively. In addition, d_c, l_c, and h_c represent the diameter, length, and thickness of CNTs, whereas w_g, l_g, and h_g denote the width, length, and thickness of GPLs. The volume fraction of CNTs and GPLs is expressed as follows (Mirfatah et al., 2022):

$$V_r=\frac{W_c}{w_c+\rho_c/\rho_n\left(1-W_c\right)},\quad V_g=\frac{W_g}{W_g+\rho_g/\rho_n\left(1-W_g\right)}, \tag{3}$$

where W_c, W_g denote the mass fractions of CNTs and GPLs, respectively.

Therefore, the mechanical properties of three phase composites are described as (Mirfatah et al., 2022)

$$E_{11}^{ri}=V_FE_{11}^F+\left(1-V_F\right)E_r^i,\ G_{12}^{ri}=\left(V_F/G_{12}^F+\left(1-V_F\right)/G_r^i\right)^{-1},\ G_r^i=E_r^i/\left[2\left(1+v_r^i\right)\right],$$
$$E_{22}^{ri}=\left[\frac{V_F}{E_{22}^F}+\frac{1-V_F}{E_r^i}-V_F\left(1-V_F\right)\frac{\left(v_{12}^F\right)^2\left(E_r^i/E_{22}^F\right)+\left(v_r^i\right)^2\left(E_{22}^F/E_r^c\right)-2v_{12}^Fv_r^i}{V_FE_{22}^F+\left(1-V_F\right)E_r^i}\right]^{-1},$$
$$v_{12}^{ri}=V_Fv_{12}^F+\left(1-V_F\right)v_r^i,\quad v_{21}^{ri}=\frac{E_{22}^{ri}}{E_{11}^{ri}}v_{12}^{ri},\quad \rho_{ri}=V_F\rho_F+\left(1-V_F\right)\rho_r^i, \tag{4}$$
$$\alpha_{11}^{ri}=\frac{V_FE_{11}^F\alpha_{11}^F+\left(1-V_F\right)E_r^i\alpha_r^i}{V_FE_{11}^F+\left(1-V_F\right)E_r^i},\quad \alpha_{22}^{ri}=\left(1+v_{12}^F\right)V_F\alpha_{22}^F+\left(1+v_r^i\right)\left(1-V_F\right)\alpha_r^i-v_{12}^{ri}\alpha_{11}^{ri},$$

in which E_{11}^F, E_{22}^F, G_{12}^F, ρ_F, and ν_{12}^F are the elastic moduli, shear modulus, density, and Poisson's ratio of the fibers, respectively. The superscripts *rc* and *rg* denote the fiber-reinforced polymer matrix composite and the nanocomposites reinforced with CNTs and GPLs, respectively.

The electromagnetic face layers are composed of a mixture of Barium Titanate ($BaTiO_3$) and Cobalt Ferrite ($CoFe_2O_4$). In this study, the volume fraction of $BaTiO_3$-$CoFe_2O_4$ mixture in each layer is taken as 0.5, and the corresponding material properties are adopted from Van Huong et al. (2024).

2.2. Governing equations

Based on FSDT, the displacement field of the shell is presented as (Nguyen et al., 2020)

$$\begin{aligned} u(x,y,z,t) &= u_0(x,y,t) + z\phi_x(x,y,t), \\ v(x,y,z,t) &= v_0(x,y,t) + z\phi_y(x,y,t), \\ w(x,y,z,t) &= w_0(x,y,t), \end{aligned} \tag{5}$$

where u, v, and w are the displacement components in the x, y, and z directions, respectively; ϕ_x and ϕ_y denote the rotations of the normal to the mid-surface about the y- and x-axes, respectively; and t is the time. The strain components are defined as follows (Nguyen et al., 2020):

$$\begin{bmatrix} \varepsilon_x \\ \varepsilon_y \\ \gamma_{xy} \end{bmatrix} = \begin{bmatrix} \varepsilon_x^0 \\ \varepsilon_y^0 \\ \gamma_{xy}^0 \end{bmatrix} + z \begin{bmatrix} \phi_{x,x} \\ \phi_{y,y} \\ \phi_{x,y} + \phi_{y,x} \end{bmatrix}, \begin{bmatrix} \gamma_{xz} \\ \gamma_{yz} \end{bmatrix} = \begin{bmatrix} w_{,x} + \phi_x \\ w_{,y} + \phi_y \end{bmatrix}, \begin{bmatrix} \varepsilon_x^0 \\ \varepsilon_y^0 \\ \gamma_{xy}^0 \end{bmatrix} = \begin{bmatrix} u_{0,x} - w_0/R_x + 0.5(w_{0,x})^2 \\ v_{0,y} - w_0/R_y + 0.5(w_{0,y})^2 \\ u_{0,y} + v_{0,x} + w_{0,x}w_{0,y} \end{bmatrix}, \tag{6}$$

in which ε_x and ε_y is normal strain; γ_{xy}, γ_{xz}, and γ_{yz} is the shear strain; $\varepsilon_x^0, \varepsilon_y^0, \gamma_{xy}^0, u_0, v_0, w_0$ are the strain and the displacement components at the middle surface of the shell.

The stress-strain relations of the core layer (symbol is "co") are determined by Hooke's law

$$\begin{aligned} \sigma_x^{co} &= Q_{11}^{co}\varepsilon_x + Q_{12}^{co}\varepsilon_y - (\alpha_{11}Q_{11}^{co} + \alpha_{22}Q_{12}^{co})\,\Delta T, \quad \sigma_{yz}^{co} = Q_{44}^{co}\gamma_{yz}, \\ \sigma_y^{co} &= Q_{12}^{co}\varepsilon_x + Q_{22}^{co}\varepsilon_y - (\alpha_{11}Q_{12}^{co} + \alpha_{22}Q_{22}^{co})\,\Delta T, \quad \sigma_{xz}^{co} = Q_{55}^{co}\gamma_{xz}, \quad \sigma_{xy}^{co} = Q_{66}^{co}\gamma_{xy}, \end{aligned} \tag{7}$$

The stress-strain relations of the electromagnetic layers (symbol is "f") are as follows:

$$\begin{aligned} &\sigma_x^f = \bar{C}_{11}\varepsilon_{xx}^f + \bar{C}_{12}\varepsilon_{yy}^f - \bar{e}_{31}E_z - \bar{q}_{31}H_z - \bar{\alpha}_1\Delta T, \quad \sigma_y^f = \bar{C}_{12}\varepsilon_{xx}^f + \bar{C}_{22}\varepsilon_{yy}^f - \bar{e}_{32}E_z - \bar{q}_{32}H_z - \bar{\alpha}_2\Delta T, \\ &\tau_{xy}^f = \bar{C}_{66}\gamma_{xy}^f, \quad \tau_{yz}^f = 2\sigma_{yz}^f = \bar{C}_{44}\gamma_{yz}^f - \bar{e}_{24}E_y - \bar{q}_{24}H_y, \quad \tau_{xz}^f = 2\sigma_{xz}^f = \bar{C}_{55}\gamma_{xz}^f - \bar{e}_{15}E_x - \bar{q}_{15}H_x, \end{aligned} \tag{8}$$

$$\begin{aligned} D_x^f &= \bar{e}_{15}\gamma_{xz}^f + \bar{\eta}_{11}E_x + \bar{m}_{11}H_x, \quad D_y^f = \bar{e}_{24}\gamma_{yz}^f + \bar{\eta}_{22}E_y + \bar{m}_{22}H_y, \\ D_z^f &= \bar{e}_{31}\varepsilon_{xx}^f + \bar{e}_{32}\varepsilon_{yy}^f + \bar{\eta}_{33}E_z + \bar{m}_{33}H_z, \quad B_x^f = \bar{q}_{15}\gamma_{xz}^f + \bar{m}_{11}E_x + \bar{\mu}_{11}H_x, \\ B_y^f &= \bar{q}_{24}\gamma_{yz}^f + \bar{m}_{22}E_y + \bar{\mu}_{22}H_y, \quad B_z^f = \bar{q}_{31}\varepsilon_{xx}^f + \bar{q}_{32}\varepsilon_{yy}^f + \bar{m}_{33}E_z + \bar{\mu}_{33}H_z, \end{aligned} \tag{9}$$

where $Q_{ij}^{co}, \bar{C}_{ij}\,(ij = 11, 12, 22, 44, 55, 66), \bar{e}_{ij}, \bar{q}_{ij}\,(ij = 31, 32, 15, 24), E_i, H_i\,(i = x, y, z), \Delta T, \bar{\eta}_{ij}, \bar{m}_{ij}, \bar{\mu}_{ij}\,(ij = 11, 22, 33)$ are defined in Van Huong et al. (2024).

The nonlinear governing equations of motion for the shell based on the FSDT are given as follows (Van Huong et al., 2024):

$$N_{x,x} + N_{xy,y} = I_0\ddot{u}_0 + I_1\ddot{\phi}_x, \tag{10a}$$

$$N_{xy,x} + N_{y,y} = I_0\ddot{v}_0 + I_1\ddot{\phi}_y, \tag{10b}$$

$$M_{x,x} + M_{xy,y} - Q_x = I_2\ddot{\phi}_x + I_1\ddot{u}_0, \tag{10c}$$

$$M_{xy,x} + M_{y,y} - Q_y = I_2\ddot{\phi}_y + I_1\ddot{v}_0, \tag{10d}$$

$$\begin{aligned} &Q_{x,x} + Q_{y,y} + N_x\ddot{w}_{0,xx} + 2N_{xy}\ddot{w}_{0,xy} + N_y\ddot{w}_{0,yy} - k_1w_0 \\ &\quad + k_2\left(\ddot{w}_{0,xx} + \ddot{w}_{0,yy}\right) + \frac{N_x}{R_x} + \frac{N_y}{R_y} + N_a\ddot{w}_{0,xx} = I_0\ddot{w}_0, \end{aligned} \tag{10e}$$

$$\int_{z_0}^{z_1}\left[\cos(\beta z_b)D_{x,x}+\cos(\beta z_b)D_{y,y}+\beta\sin(\beta z_b)D_z\right]\mathrm{d}z + \int_{z_2}^{z_3}\left[\cos(\beta z_t)D_{x,x}+\cos(\beta z_t)D_{y,y}+\beta\sin(\beta z_t)D_z\right]\mathrm{d}z=0, \tag{10f}$$

$$\int_{z_0}^{z_1}\left[\cos(\beta z_b)B_{x,x}+\cos(\beta z_b)B_{y,y}+\beta\sin(\beta z_b)B_z\right]\mathrm{d}z + \int_{z_2}^{z_3}\left[\cos(\beta z_t)B_{x,x}+\cos(\beta z_t)B_{y,y}+\beta\sin(\beta z_t)B_z\right]\mathrm{d}z=0, \tag{10g}$$

in which $I_i=\int_{z_0}^{z_1}\rho^f z^i\mathrm{d}z+\int_{z_1}^{z_2}\rho^{co}z^i\mathrm{d}z+\int_{z_2}^{z_3}\rho^f z^i\mathrm{d}z$, $(i=0,1,2)$ and $q\,(t)$ is the uniformly distributed external pressure on the surface of the double curved shallow sandwich shell, N_a is the axial vibration compression load; $z_b=z+\frac{h_1}{2}+\frac{h_2}{2}, z_t=z-\frac{h_1}{2}-\frac{h_2}{2}, z_0=-h_1-\frac{h_2}{2}, z_1=-\frac{h_2}{2}, z_2=\frac{h_2}{2}, z_3=h_1+\frac{h_2}{2}$. The expressions for internal force N_x, N_y, N_{xy}, moment M_x, M_y, M_{xy} and shear force Q_x, Q_y of the shell as follows (Van Huong et al., 2024).

Eqs. (10) can be solved by applying the Galerkin's method (Van Huong et al., 2024) to obtain Eqs. (11)

$$p_{11}W+p_{12}\Phi_x+p_{13}\Phi_y+p_{14}W^2+p_{15}W^3+p_{16}W\Phi_x+p_{17}W\Phi_y+p_{18}+p_{19}N_aW-I_0\ddot{W}=0, \tag{11a}$$

$$p_{21}W+p_{22}\Phi_x+p_{23}\Phi_y+p_{24}W^2+p_{25}-\rho_1\ddot{\Phi}_x=0, \tag{11b}$$

$$p_{31}W+p_{32}\Phi_x+p_{33}\Phi_y+p_{34}W^2+p_{35}-\rho_1\ddot{\Phi}_y=0, \tag{11c}$$

in which

$$\begin{aligned}&p_{11}=G_1+G_4,\ p_{12}=G_2,\ p_{13}=G_3,\ p_{14}=G_5+G_8+G_9,\ p_{15}=G_{10},\ p_{16}=G_6,\ p_{17}=G_7,\\&p_{18}=G_{11},\ p_{19}=-{\lambda_m}^2,\ p_{21}=G_{21}+G_{24},\ p_{22}=G_{22},\ p_{23}=G_{23},\ p_{24}=G_{25},\ p_{25}=G_{26},\\&\rho_1=I_2-{I_1}^2/I_0,\ p_{31}=G_{31}+G_{34},\ p_{32}=G_{32},\ p_{33}=G_{33},\ p_{34}=G_{35},\ p_{35}=G_{36},\end{aligned} \tag{12}$$

and $G_{ij}\,(i=1,2,\ldots,11,21,22,23,24,25,26,31,32,34,35,36)$, I_0, I_1, I_2, λ_m are found in Van Huong et al. (2024).

2.3. Dynamic stability analysis

Eq. (11) can be reformulated in the following form:

$$\mathbf{P}\cdot\boldsymbol{\chi}+P_{cr}\left(\mu_{1s}+\mu_{1d}\cos\theta t\right)\cdot\mathbf{M}\cdot\boldsymbol{\chi}+\mathbf{H}-\mathbf{I}\cdot\frac{\partial^2\boldsymbol{\chi}}{\partial t^2}=0, \tag{13}$$

where $N_a=P_{cr}\left(\mu_{1s}+\mu_{1d}\cos\theta t\right)$, P_{cr} is the buckling load, and μ_{1s} and μ_{1d} are the static and dynamic load parameters, respectively, and

$$\mathbf{P}=\begin{bmatrix}p_{11}&p_{12}&p_{13}\\p_{21}&p_{22}&p_{23}\\p_{31}&p_{32}&p_{33}\end{bmatrix},\quad \boldsymbol{\chi}=\begin{bmatrix}W\\\Phi_x\\\Phi_y\end{bmatrix},\quad \mathbf{M}=\begin{bmatrix}p_{19}&0&0\\0&0&0\\0&0&0\end{bmatrix},$$
$$\mathbf{I}=\begin{bmatrix}I_0&0&0\\0&\rho_1&0\\0&0&\rho_1\end{bmatrix},\quad \mathbf{H}=\begin{bmatrix}p_{18}\\p_{25}\\p_{35}\end{bmatrix}, \tag{14}$$

Solving Eq. (14) gives the natural frequencies ω (rad/s) of the shell as

$$\det\left|\mathbf{P}+\mathbf{I}\omega^2\right|=0. \tag{15}$$

Solving Eq. (13) gives the buckling load of the shell as

$$\det\left|\mathbf{P}+P_{cr}\mathbf{M}\right|=0. \tag{16}$$

Instabilities occur only within specific regions of the frequency–excitation amplitude plane, where the boundaries of these unstable zones correspond to periodic solutions of the governing equations of motion. The periodic solution of Eq. (13) with period $2T_0$ ($T_0=2\pi/\theta$) can be expressed in the form of a trigonometric series based on Bolotin's first approximation method (Bolotin, 1964)

$$\chi=\sum_{k=1,3,\ldots}^{\infty}\left[a_k\sin\left(k\frac{\theta t}{2}\right)+b_k\cos\left(k\frac{\theta t}{2}\right)\right], \tag{17}$$

where a_k and b_k are arbitrary constant parameters. Because the first-order approximate solution provides sufficient accuracy $k=1$, a conservative estimate of the primary unstable region can be obtained. In the case of periodic axial loading with a single excitation frequency, this first unstable (fundamental) region is therefore identified.

Differentiating a one-term solution twice with respect to time yields

$$\ddot{\chi}=-a_1\frac{\theta^2}{4}\sin\frac{\theta t}{2}-b_1\frac{\theta^2}{4}\cos\frac{\theta t}{2}, \tag{18}$$

Substituting χ and $\ddot{\chi}$ into Eq. (13), simplifying the trigonometric relations, and then comparing the coefficients of $\sin\dfrac{\theta t}{2}$ and $\cos\dfrac{\theta t}{2}$ gives two algebraic matrix equations for a_1 and b_1

$$\left[\mathbf{P}+P_{cr}\mathbf{M}\left(\mu_{1s}+\frac{1}{2}\mu_{1d}\right)+\mathbf{I}\frac{\theta^2}{4}\right]a_1=0,\quad \left[\mathbf{P}+P_{cr}\mathbf{M}\left(\mu_{1s}-\frac{1}{2}\mu_{1d}\right)+\mathbf{I}\frac{\theta^2}{4}\right]b_1=0. \tag{19}$$

The excitation frequencies θ can be determined from Eqs. (19) for a prescribed dynamic load by applying standard eigenvalue solution procedures, as follows:

$$\det\left|\mathbf{P}+P_{cr}\mathbf{M}\left(\mu_{1s}+\frac{1}{2}\mu_{1d}\right)+\mathbf{I}\frac{\theta^2}{4}\right|=0,\quad \det\left|\mathbf{P}+P_{cr}\mathbf{M}\left(\mu_{1s}-\frac{1}{2}\mu_{1d}\right)+\mathbf{I}\frac{\theta^2}{4}\right|=0. \tag{20}$$

3. COMPARISON STUDIES

To verify the accuracy of the present formulation, Table 1 compares the dimensionless natural frequencies $\bar{\omega}=\omega_{mn}a\sqrt{\rho/G}$ of the shell with the results reported by Dawe and Roufaeil (1980). The selected parameters are $a=b$, $h=0.1\,\mathrm{m}$, $E=10\,920\,\mathrm{Pa}$, $v=0.3$, and $G=E/[2(1+v)]$. In addition, using the material parameters given in (Shooshtari & Razavi, 2016), the dimensionless frequencies $\bar{\omega}=\omega_{mn}a\sqrt{\rho_0/C_{11}}$ of a magneto-electro-elastic plate with various length-to-thickness ratios are presented in Table 2 ($k_1=k_2=0$, $\phi_0=\psi_0=0$, $h=1\,\mathrm{mm}$). The results show very good agreement with previously published studies, demonstrating the reliability and accuracy of the present approach.

Table 1. Dimensionless frequency comparison of square plate

h/a	Dawe and Roufaeil (1980)	Present
0.01	0.0963	0.09634
0.1	0.93	0.9376

Table 2. Comparison of dimensionless frequencies of a magneto electro elastic square plate

Mode (m,n)	Method	a/h	
		50	100
(1, 1)	HSDT (Shooshtari & Razavi, 2016)	0.1131	0.0566
	C^0-HSDT (Hung et al., 2023)	0.1135	0.0567
	Present	0.1074	0.0539
(1, 2)	HSDT (Shooshtari & Razavi, 2016)	0.2792	0.1402
	C^0-HSDT (Hung et al., 2023)	0.2803	0.1408
	Present	0.2730	0.1375
(2, 2)	HSDT (Shooshtari & Razavi, 2016)	0.4492	0.2261
	C^0-HSDT (Hung et al., 2023)	0.4507	0.2271
	Present	0.4251	0.2148

4. NUMERICAL RESULT AND DISCUSSION

This section examines the dynamic response of a double curved shallow shell subjected to external loads located either inside or outside the dynamic instability region (DIR). The parameters used consistently in this section: Core-reinforced nanocomposite materials are GPLs, $a = b$, $b = 10h$, $h = 0.1\,\text{m}$, $\phi_0 = 400\,\text{V}$, $\psi_0 = 200\,\text{A}$, $k_1 = 1\,\text{GPa/m}$, $k_2 = 0.02$ GPa.m, $R_x = R_y = a/0.5$, $\Delta T = 50\,\text{K}$, $W_g = W_c = 8\%$, $V_F = 15\%$. The DIR is shown in Fig. 2 for the parameters $P_{cr} = 5.9846 \times 10^8\ \text{N/m}^2$ and $\mu_{1s} = 1$. Four representative cases corresponding to different combinations of μ_{1d} and θ, denoted as points A, B, C, and D in Fig. 2, are analyzed. Points C and D lie within the DIR, and point A lies outside the DIR (stable region), while point B is situated on the boundary of the DIR.

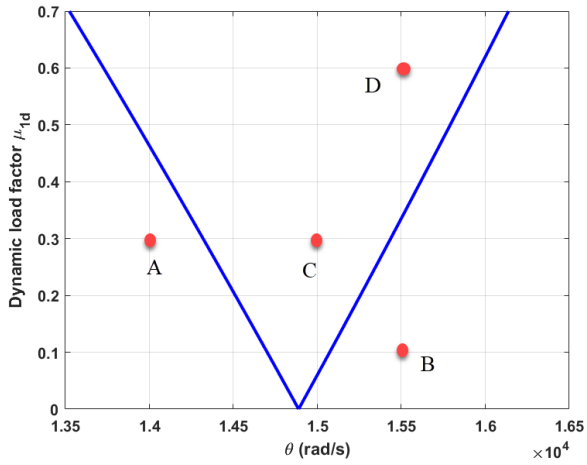

Fig. 2. Dynamic instability region (DIR) of the DSEM shell with a nanocomposite core

Fig. 3 presents the nonlinear displacement-time responses of the shell under four representative loading cases. When the applied load lies within the dynamic instability region (points C and D), the oscillation amplitude grows significantly with time, indicating strong fluctuations. This behavior is attributed to resonance, which amplifies the shell's vibratory response. In contrast, when the loading parameters lie outside the DIR (points A and B), the oscillation amplitude remains finite and stable, demonstrating that no resonance occurs in the stable region.

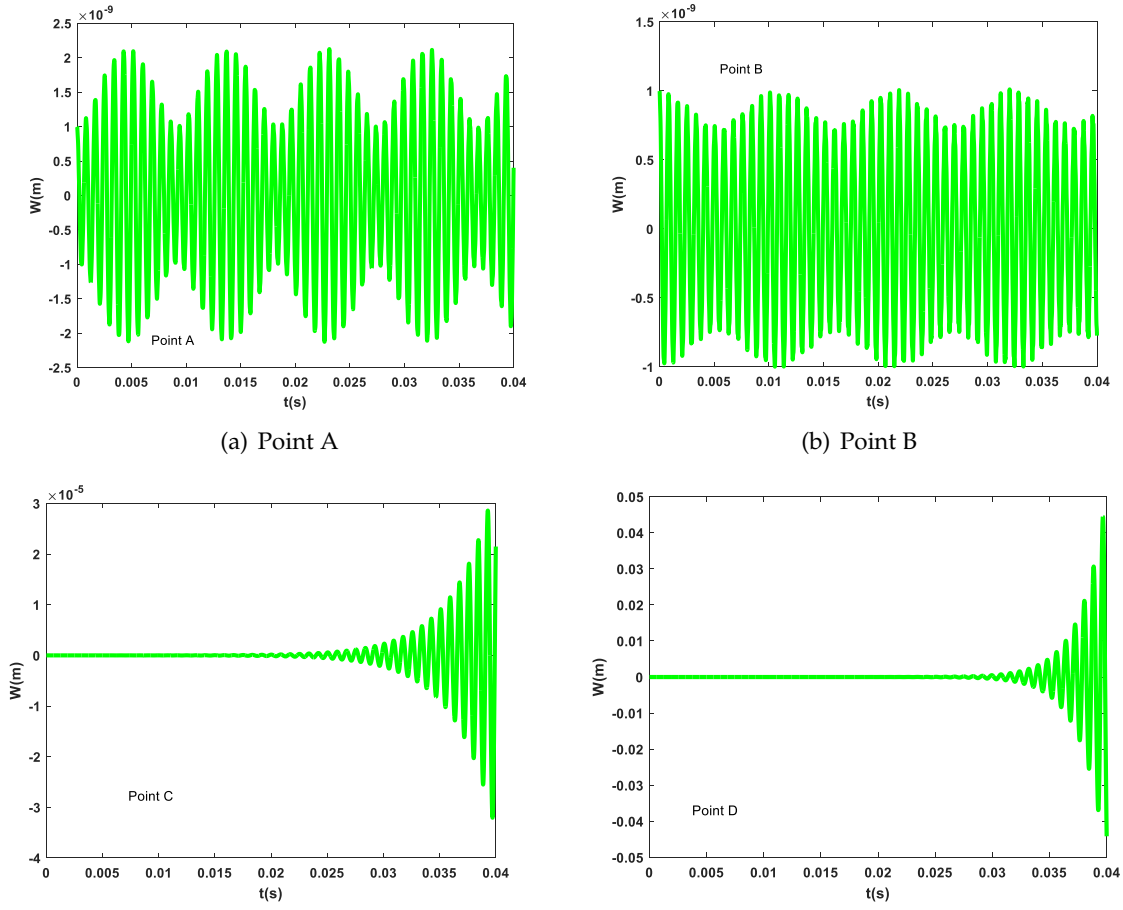

(a) Point A (b) Point B

(c) Point C (d) Point D

Fig. 3. Time–deflection responses of the DSEM shell under different load cases

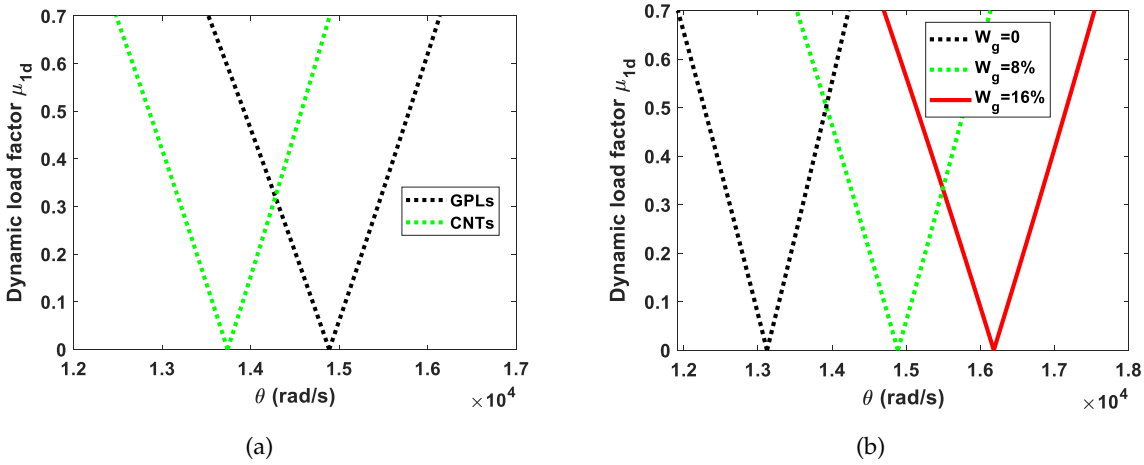

(a) (b)

Fig. 4. Effect of core-reinforcement material models (a) and the mass fraction of graphene (b) on the DIR of the DSEM shell

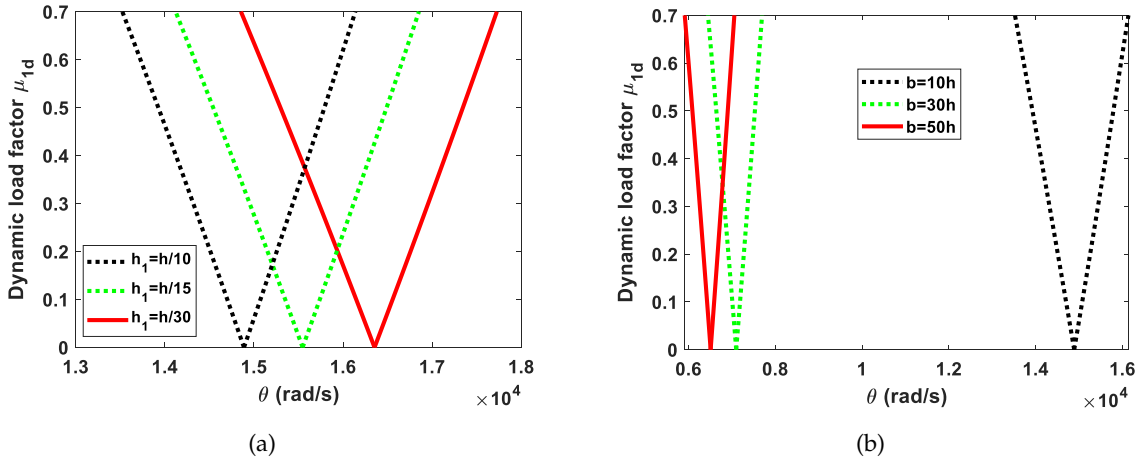

Fig. 5. Effect of electromagnetic layer thickness ratios and width-to-thickness ratio on the DIR of the DSEM shell

Fig. 4 illustrates the influence of two core-reinforcement material models and the mass fraction of graphene on the DIR of the DSEM shell. The general shape of the DIR remains similar for different reinforcement types, however the excitation frequencies associated with GPLs are consistently higher than those for CNTs. This trend arises from the fact that GPLs possess a higher Young's modulus than CNTs, resulting in greater shell stiffness and hence higher excitation frequencies. Likewise, increasing the mass fraction of graphene enhances the stiffness of the core, which also shifts the excitation frequency upward.

Fig. 5(a) shows the influence of the electromagnetic layer thickness ratios on the DIR of the DSEM shell. As illustrated, decreasing the thickness of the piezoelectric layer results in higher excitation frequencies, while the overall shape of the instability region remains essentially unchanged. Fig. 5(b) demonstrates that increasing the width-to-thickness ratio leads to a reduction in the excitation frequency and shifts the DIR toward lower frequency values. The reason is that a higher width-to-thickness ratio corresponds to a thinner shell, which decreases the overall stiffness of the structure.

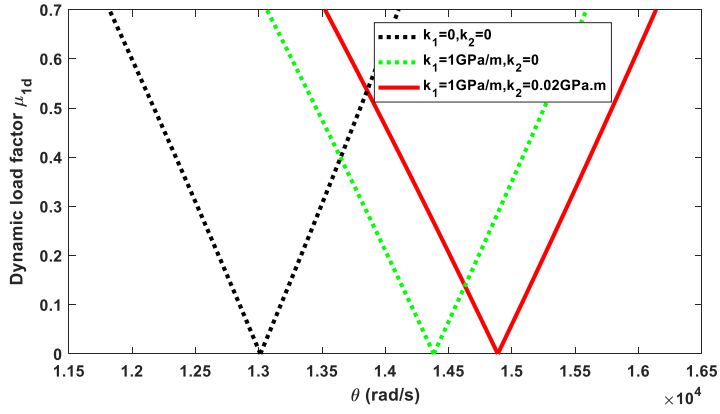

Fig. 6. Impact of elastic foundation parameters on the DIR of the DSEM shell

Fig. 6 evaluates the influence of the Winkler and Pasternak elastic foundation parameters by considering $k_1 = 0$ and $k_1 = 1\,\mathrm{GPa/m}$, and $k_2 = 0$ and $k_2 = 0.02$ GPa.m, respectively. The results show that increasing either k_1 or k_2 leads to higher excitation frequencies, thereby shifting

the DIR toward larger frequency values. This behavior indicates that both the Winkler and Pasternak foundation models effectively enhance the stiffness of the shell.

5. CONCLUSIONS

The excitation frequency of the multilayer double curved sandwich electromagnetic shell is strongly influenced by both its material characteristics and geometric parameters. The results show that employing GPL-reinforced core, decreasing the width-to-thickness ratio, and reducing the thickness of the electromagnetic layers all lead to an increase in excitation frequency. Moreover, as the volume fraction of CNTs or GPLs increases, the stiffness of the shell improves, causing the instability region to shift consistently toward higher excitation frequencies.

DECLARATION OF COMPETING INTEREST

The authors declare that they have no known competing financial interests or personal relationships that could have appeared to influence the work reported in this paper.

CREDIT AUTHOR STATEMENT

Pham Hong Cong: *Conceptualization, Methodology, Software, Writing – original draft*. Nguyen Van Huong: *Investigation, Validation, Writing – original draft*. Nguyen Dinh Duc: *Methodology, Supervision*. Trinh Minh Chien: *Writing – review & editing*.

ACKNOWLEDGEMENT

This research was supported by the Vietnam Academy of Science and Technology under Grant No. VAST01.01/25-26.

REFERENCES

Anh, V. T. T., Khoa, N. D., Ngo, T., & Duc, N. D. (2023). Vibration of hybrid eccentrically stiffened sandwich auxetic double curved shallow shells in thermal environment. *Aerospace Science and Technology*, *137*, 108277. https://doi.org/10.1016/j.ast.2023.108277

Bolotin, V. V. (1964). *The dynamic stability of elastic systems*. Holden-Day, Inc.

Chakraborty, S., Dey, T., & Kumar, R. (2021). Instability characteristics of damped CNT reinforced laminated shell panels subjected to in-plane excitations and thermal loading. *Structures*, *34*, 2936–2949. https://doi.org/10.1016/j.istruc.2021.09.047

Cong, P. H., Huong, N. V., Thien, T. T., & Duc, N. D. (2024). Nonlocal strain gradient-based geometrically nonlinear vibration analysis of double curved shallow nanoshell containing functionally graded layers. *Aerospace Science and Technology*, *151*, 109310. https://doi.org/10.1016/j.ast.2024.109310

Dawe, D., & Roufaeil, O. (1980). Rayleigh–Ritz vibration analysis of Mindlin plates. *Journal of Sound and Vibration*, *69*(3), 345–359. https://doi.org/10.1016/0022-460x(80)90477-0

Feng, J., Wu, Y., Xue, J., & Lin, J. (2024). Dynamic stability analysis of laminated cylindrical shells considering fluid–structure interaction. *Composite Structures*, *340*, 118183. https://doi.org/10.1016/j.compstruct.2024.118183

Hung, P., Thai, C. H., & Phung-Van, P. (2023). A C0-HSDT free vibration of magneto-electro-elastic functionally graded porous plates using a moving Kriging meshfree method. *Aerospace Science and Technology*, *137*, 108266. https://doi.org/10.1016/j.ast.2023.108266

Jahangiri, R., Rezaee, M., & Manafi, H. (2022). Nonlinear and chaotic vibrations of FG double curved sandwich shallow shells resting on visco-elastic nonlinear Hetenyi foundation under combined resonances. *Composite Structures*, *295*, 115721. https://doi.org/10.1016/j.compstruct.2022.115721

Mirfatah, S. M., Tayebikhorami, S., Shahmohammadi, M. A., Salehipour, H., & Civalek, Ö. (2022). Thermo-elastic damped nonlinear dynamic response of the initially stressed hybrid GPL/CNT/fiber/polymer composite toroidal shells surrounded by elastic foundation. *Composite Structures*, *283*, 115047. https://doi.org/10.1016/j.compstruct.2021.115047

Nguyen, D. D., Kim, S.-E., Vu, T. A. T., & Vu, A. M. (2020). Vibration and nonlinear dynamic analysis of variable thickness sandwich laminated composite panel in thermal environment. *Journal of Sandwich Structures & Materials*, *23*(5), 1541–1570. https://doi.org/10.1177/1099636219899402

Sayyad, A. S., Ghugal, Y. M., & Kant, T. (2023). Higher-order static and free vibration analysis of doubly-curved FGM sandwich shallow shells. *Forces in Mechanics*, *11*, 100194. https://doi.org/10.1016/j.finmec.2023.100194

Shooshtari, A., & Razavi, S. (2016). Vibration analysis of a magnetoelectroelastic rectangular plate based on a higher-order shear deformation theory. *Latin American Journal of Solids and Structures*, *13*(3), 554–572. https://doi.org/10.1590/1679-78251831

Thi, T. H. N., Tran, V. K., Tu, P. H., & Thao, P. H. (2025). Dynamic instability analysis of piezoelectric fluid-infiltrated porous metal foam nanosheet considering surface and flexoelectricity effects in hygro-thermal environment. *International Journal of Mechanics and Materials in Design*, *21*(2), 261–296. https://doi.org/10.1007/s10999-024-09736-2

Tu, P. H., Van Ke, T., Trai, V. K., & Hoai, L. (2024). An isogeometric analysis approach for dynamic response of doubly-curved magneto electro elastic composite shallow shell subjected to blast loading. *Defence Technology*, *41*, 159–180. https://doi.org/10.1016/j.dt.2024.06.005

Van Huong, N., Cong, P. H., & Duc, N. D. (2024). Nonlinear vibration analysis of a double curved shallow sandwich shell in which the core made of three-phase nanocomposite and the two-outer layer of electromagnetic materials. *Thin-Walled Structures*, *196*, 111501. https://doi.org/10.1016/j.tws.2023.111501

Yadav, A., Amabili, M., Panda, S. K., & Dey, T. (2023). Instability analysis of fluid-filled angle-ply laminated circular cylindrical shells subjected to harmonic axial loading. *European Journal of Mechanics - A/Solids*, *97*, 104810. https://doi.org/10.1016/j.euromechsol.2022.104810

Yadav, A., Amabili, M., Panda, S., Dey, T., & Kumar, R. (2022). A semi-analytical approach for instability analysis of composite cylindrical shells subjected to harmonic axial loading. *Composite Structures*, *296*, 115882. https://doi.org/10.1016/j.compstruct.2022.115882

Zaidan, S. M., & Hasan, H. M. (2023). Influences of angular velocity and periodic axial load on the dynamic instability of functionally graded porous cylindrical panels. *Archive of Applied Mechanics*, *93*(7), 2793–2812. https://doi.org/10.1007/s00419-023-02407-2